The Influence of Absorber Thickness on $Cu(In,Ga)Se_2$ Solar Cells With Different Buffer Layers

Jonas Pettersson, Tobias Törndahl, Charlotte Platzer-Björkman, Adam Hultqvist, and Marika Edoff

***Abstract*—This study investigates the interplay between the absorber layer of $Cu(In,Ga)Se_2$ solar cells and the other layers of these devices. $Cu(In,Ga)Se_2$ devices with absorbers of different thicknesses and different buffer layers are fabricated. Absorber layers and finished devices are characterized. Good efficiencies are obtained, also for devices of substandard thickness down to 0.3 μm. Best open-circuit voltages and fill factors are found for cells with half the standard absorber thickness, but the highest efficiencies are found for cells with the standard thickness of 1.6 μm due to their higher short-circuit current density. $Cu(In,Ga)Se_2$ cells with Zn(O,S) buffer layers are more efficient than CdS reference devices for the same absorber thickness due to a higher short-circuit current. For cells with thin absorber layers, a part of the higher current is caused by higher quantum efficiency at long wavelengths. Electrical simulations indicate that the loss in the open-circuit voltage for the thinnest devices is due to recombination in the back contact region. The difference in long-wavelength quantum efficiency between the buffer layers is attributed to a difference in the CIGS band bending. Acceptors at the $Cu(In,Ga)Se_2$–CdS interface are proposed as an explanation for this difference. A low-quality back contact region enhances the effect.**

***Index Terms*—Photovoltaic cells, semiconductor device modeling.**

I. Introduction

THIN absorber, $Cu(In,Ga)Se_2$, CIGS, solar cells with CdS buffer layers have been studied experimentally by a number of authors [1]–[5]. The common conclusion of these studies has been that the cell efficiency stayed on a high level down to a CIGS layer thickness of about 1 μm. Below this thickness there is a severe degradation of the efficiency due to sharp losses in short-circuit current density J_{sc}, open-circuit voltage V_{oc}, and in some cases fill factor (FF). These reductions were attributed to optical losses, increase in recombination due to the degradation of the CIGS material, back contact recombination, and shunting problems. An electron reflector due to more Ga close to the back contact was found to give some improvement of the devices [1], [3]. In some studies, optical [3], [6]–[9] and electrical [10] modeling have been applied. These studies suggested different ways to improve thin CIGS cells. The back contact could be improved by increasing the total optical reflection as well as by increasing the diffuse reflectance using texturing. The introduction of an electron reflector at the back contact to avoid recombination was also suggested. Other proposals were to texture the front contact in such a way that an antireflective layer is created and to use a buffer layer with a higher band gap than CdS to minimize light absorption there. The main objective of previous studies was to investigate the potential of thinner, less material consuming, and thereby cheaper devices. In this study, devices with CIGS thickness between 0.3 and 1.6 μm are fabricated and characterized in order to understand more about the interplay between the different layers and interfaces. The experimental work is accompanied by device modeling in solar cell capacitance simulator (SCAPS) [11]. An important part of this study is the comparison of cells with chemical bath deposited CBD–CdS buffer layers with devices that have Zn(O,S) buffer layers from atomic layer deposition (ALD) [12]. The fabricated cells have a continuously increasing Ga/In+Ga ratio in the CIGS-layer, toward the back contact. This band gap gradient is accounted for in electrical modeling that is based on compositional measurements.

II. Experimental Setup

A. Sample Processing

The solar cells have a soda-lime-glass/Mo/CIGS/buffer layer/undoped ZnO/ZnO:Al/metal grid stack and an area of approximately 0.5 cm^2. An in-house developed baseline recipe was followed for the glass cleaning, the dc-sputtering of molybdenum, the radio-frequency sputtering of ZnO, and the electron-beam evaporation of the Ni/Al/Ni metal grid [13]. In this study, both CBD–CdS and ALD–Zn(O,S) are used as buffer layers. The CdS layer thickness is usually between 50 and 70 nm, while the Zn(O,S) buffer layer thickness has been estimated to 25 nm [14].

The CIGS films in this study were deposited by co-evaporation in an inline evaporator, where the substrates passed in front of three stationary sources of gallium, indium, and copper, respectively [15]. During film deposition, the three sources delivered a constant rate of evaporated material together with a nondirectional selenium source that provides a background partial pressure in the evaporator. As a result of the positioning

Manuscript received February 28, 2013; revised May 8, 2013 and June 24, 2013; accepted July 23, 2013. Date of publication August 15, 2013; date of current version September 18, 2013. This work was supported in part by the Swedish Energy Agency and in part by the Göran Gustafsson Foundation.

J. Pettersson, T. Törndahl, C. Platzer-Björkman, and M. Edoff are with the Ångström Solar Center, Division of Solid State Electronics, Uppsala University, Uppsala SE-751 21, Sweden (e-mail: jonasgp81@gmail.com; tobias.torndahl@angstrom.uu.se; charlotte.platzer@angstrom.uu.se; marika.edoff@angstrom.uu.se).

A. Hultqvist is with the Department of Chemical Engineering, Stanford University, Stanford, CA 94305 USA (e-mail: adamhq@stanford.edu).

Color versions of one or more of the figures in this paper are available online at http://ieeexplore.ieee.org.

Digital Object Identifier 10.1109/JPHOTOV.2013.2276030

TABLE I
SOLAR CELL SAMPLES STUDIED IN THIS STUDY

Sample	Buffer type	CIGS thickness (Profilometer) [μm]	GGI (XRF) [%]	CGI (XRF) [%]
ZnOSx1	Zn(O,S)	1.5-1.7	45	92
CdSx1	CdS	1.5-1.7	45	92
ZnOSx1/2	Zn(O,S)	0.8-0.9	46	90
CdSx1/2	CdS	0.8-0.9	46	90
ZnOSx1/6	Zn(O,S)	0.3	46	87
CdSx1/6	CdS	0.3	46	87

of the metal sources the CIGS films are graded with an increasing [Ga]/([In]+[Ga]), GGI, content toward the Mo back contact. During CIGS growth, the substrates passed three regions in the evaporator, one heat-up zone, one deposition zone, and one cool down zone, where the substrate time in the deposition zone was approximately 20 min for a standard CIGS process. For this series, three samples were made, one with the standard process and two thinner samples by increasing the speed of the substrates in the deposition zone by two and six times while leaving the substrate speed in the other zones unchanged. The deposition temperature was estimated to be around 550 °C at the end of the deposition zone by measuring the temperature at the backside of the soda lime glass substrates by two pyrometers.

The deposition of the Zn(O,S) buffer layers was performed in a homebuilt ALD system at 120 °C using H_2O, H_2S, and diethyl zinc (DEZ), as the precursors for O, S, and Zn, respectively [14]. In this study, a DEZ/N_2/H_2O/N_2 growth cycle was employed with corresponding pulse times of 250/5000/500/5000 ms where every seventh growth cycle was modified to replace the H_2O pulse with a 500-ms-long H_2S pulse [14], [16]. The thickness of the undoped ZnO was 20 nm for the Zn(O,S) devices, while it was 100 nm for the CdS cells.

No further post-processing of the devices was performed.

B. Measurements

The average CIGS film composition was measured by means of X-ray fluorescence (XRF), using a Spectro X-Lab 2000 spectrometer with calibration against a standard of known composition. Each measurement was recorded over a circular sample area with a diameter of 1 cm. The resulting values of the average GGI and [Cu]/([Ga]+[In]), CGI, ratios are listed in Table I.

Compositional depth profiling was performed using Ar ion sputtering with 0.5 keV energy in an XPS Quantum 2000 scanning ESCA Microprobe (from Physical Electronics, Inc.) with monochromatic Al Kα radiation. The calibration of sensitivity factors, taking into account preferential sputtering effects, was performed by measuring the same profile on a nongraded CIGS sample with metal compositions determined by XRF. The selenium content was assumed to be 50 at.%.

CIGS film thickness was determined at a few different positions on each sample that uses a profilometer. Thicknesses are displayed in Table I.

Cell samples do not show any significant metastabilities with regards to performance. Room temperature current voltage *J–V* curves were acquired in darkness and in light under a Newport Oriel Sol2A solar simulator. The output power of the lamp was calibrated separately for each sample that uses the J_{sc} value from external quantum-efficiency (EQE) measurements on one of the cells of this sample. EQE measurements were performed in ambient light at room temperature and were calibrated by means of reference cells with known spectral response. EQE measurements were performed at bias voltages from 0 down to −0.5 V.

J–V curves were also obtained in a nitrogen-cooled cryostat at temperatures from 150 to 330 K, in 10 K steps. During light *J–V* measurements, cells were illuminated with the Sol2A simulator.

Capacitance voltage (*CV*) profiles were recorded in darkness in the cryostat at the same temperatures. During measurements an ac-signal with a frequency of 500 kHz and an amplitude of 30 mV was applied on the device under study. The dc-voltage was swept between 1 and −2V.

The optical characterization of solar cell stacks, which includes all layers except the contact grid, was performed. The total reflection of six samples, one for each absorber–buffer layer combination, was measured by a Perkin-Elmer λ900 dual beam spectrophotometer that is equipped with an integrating sphere. Additionally, reflection and transmission of stacks that consists of all layers except the molybdenum back contact and the front contact grid were measured. In this case, samples of the two thinner CIGS thicknesses were studied.

C. Electrical Modeling

The starting point for simulations was the baseline model established in previous modeling works [17]–[19]. The existence of a wide-gap surface defect layer (SDL), in the CIGS-layer close to the absorber–buffer interface, is a much disputed issue (see [20] and refrences therein). In our previous work, we found that measurements on cells could be well reproduced in simulations regardless of including an SDL. Only a few parameters, among them the interface defect density, had to be changed between the two cases. Therefore, for simplicity, no such wide-gap defect layer is included in this study.

Optical absorption data of the CIGS and CdS layers is based on optical constants measured by Orgassa *et al*. [21], [22]. Absorption data of ZnO (see Ref. [23]) and Zn(O,S) are obtained from reflectance-transmittance measurements conducted in the group.

Some adjustments of the model were needed to reproduce the characteristics of the devices fabricated here. Important electrical parameters used in the simulations of this paper are displayed in Table II. CIGS doping was chosen so as to give a depletion width of about 0.2 μm, similar to what was found in *CV* measurements (see Table IV). For all three CIGS-thicknesses, the GGI-ratio is modeled as linear functions between the extreme values of 0.2 at the front surface to 0.56 at the back contact. These values correspond to band gaps of about 1.1 and 1.3 eV with the bandgap calculated as

$$E_g = 1.01 + 0.626x - 0.167x(1-x) \tag{1}$$

where x is the Ga/III ratio [24], [25]. The gradings in SCAPS (see Fig. 1) are based on XPS depth profiling data.

TABLE II
SOME IMPORTANT MODELING PARAMETERS USED IN THIS STUDY

Layer Properties				
	CIGS	**Zn(O,S)**	**Zn(O,S)**	**CdS**
Thickness [μm]	1.6	0.005	0.02	0.07
	0.85	"	"	"
	0.3	"	"	"
E_g [eV]	1.11-1.32	3.0	2.7	2.4
Doping [cm^{-3}]	3×10^{16} (a)	3×10^{18} (d)	3×10^{18} (d)	5×10^{17} (d)
Properties of Deep Defects				
N [cm^{-3}]	7×10^{13}-7×10^{17} (D)	10^{16} (A)	10^{16} (A)	3×10^{17} (A)
σ_n [cm^2]	10^{-13}	10^{-15}	10^{-15}	10^{-15}
σ_p [cm^2]	10^{-15}	5×10^{-13}	5×10^{-13}	5×10^{-13}
Interface Properties				
	CIGS/Zn(O,S)	**Zn(O,S)/Zn(O,S)** (S-rich/S-poor)	**CIGS/CdS**	**CIGS/CdS** (Acc. model)
CBO [eV]	0.25	-0.4	0.24	0.24
N [cm^{-2}]	10^{11} (D)	-	3×10^{10} (D)	10^{13} (A)
σ_n [cm^2]	10^{-13}	-	10^{-13}	10^{-18}
σ_p [cm^2]	10^{-15}	-	10^{-15}	10^{-18}
E_t-$E_{V(CIGS)}$ [eV]	0.59	-	0.59	0.35
Back Contact Properties				
Φ_{bp} [eV]	S_n [cm/s]	S_p [cm/s]	Reflection [%]	
0.1	10^6	10^6	20-58 (λ-depend.)	

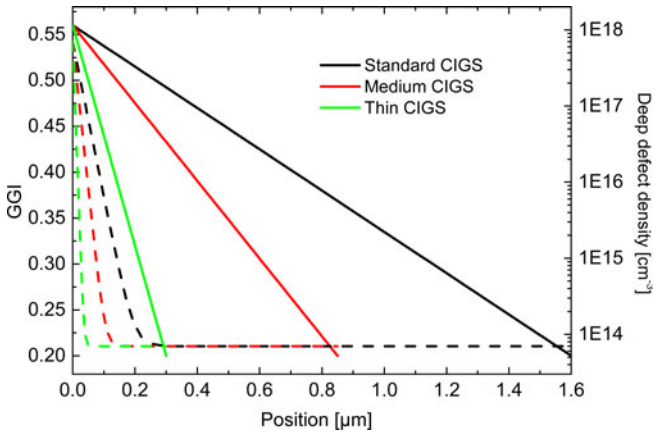

Fig. 1. Ga-grading (full) and bulk defect profiles (dashed) used in the models with CIGS layers of different thicknesses. The x-axis is defined so that the back contact lies at 0 μm. The Ga-grading profiles are linear throughout the layers, while the defect profiles consist of a constant part throughout most of the CIGS and an exponential part close to the back contact.

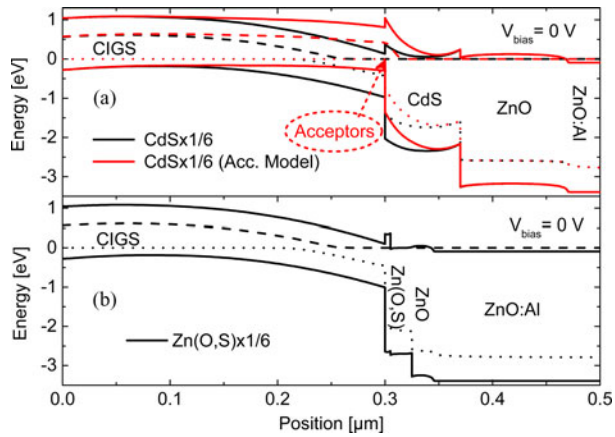

Fig. 2. Band diagrams of the three SCAPS models with 0.3 μm absorber layers. In a) the CdS models with and without interface acceptors are shown while b) depicts the Zn(O,S) model. Diagrams are calculated under illumination at zero voltage bias. Dashed and dotted lines indicate quasi-Fermi levels of electrons and holes.

Deep defect densities in the CIGS layer and at the CIGS–buffer interface were modified to reproduce trends in the measurements. Best correspondence to data is obtained when assuming a high density of defects for CIGS material with a high Ga-content. It is known that CIGS with a high Ga-ratio generally is of lower quality than low Ga CIGS [26], [27]. This degradation of the material is implemented in SCAPS as an exponential rise in defect density from $7 \times 10^{13} cm^{-3}$ to $7 \times 10^{17} cm^{-3}$. An increase in bulk defect density for high-Ga CIGS, that appears roughly exponential, was previously found by Hanna *et. al.* [26]. In the models, the rise is implemented to set in at a GGI of 0.5. As a result of the GGI profile discussed previously, a defect rich material with GGI above 0.5 is, therefore, found adjacent to the back contact and it is thicker for the thicker samples. The resulting bulk defect profiles are shown in Fig. 1.

Additionally a Schottky barrier to holes of 0.1 eV must be introduced at the back contact to reproduce the trends in V_{oc}. The properties of the molybdenum back contact is process dependent and the existence of a barrier there has been suggested by some authors of [28]. A wavelength dependent reflection at the back contact is included in the models. Back reflection was calculated according to the method of Duerinckx *et al.* [29] using the optical constants obtained by Orgassa *et al.* [21], [22]. All bulk defects are positioned at the intrinsic level, close to midgap.

Two different models of the CIGS–CdS interface are studied in this paper. These models are presented in Table II. One model includes donors, while the other model includes acceptors at the interface. The interface acceptors reduce the potential drop in the CIGS layer as seen in the zero bias band diagrams for the 0.3 μm models with CdS buffer displayed in Fig. 2(a).

In simulations, the Zn(O,S) buffer is divided into a higher band gap sulfur-rich interface layer (S/Zn = 0.7) closest to the absorber and a less sulfur containing (S/Zn = 0.3) thicker layer

TABLE III
MEASURED LIGHT-*J*–*V* SOLAR CELL PARAMETERS

Sample	**V_{oc}** [mV]	**J_{sc}** JV/IQE [mA cm^{-2}]	**FF** [%]	**η** [%]	**J_0** Light/Dark [mA cm^{-2}]	**A** Light/Dark -	**R_s** Light/Dark [Ω cm^2]	**G_{sh}** Light/Dark [mSv cm^{-2}]
ZnOSx1	680	32.9/36.4	72.1	16.1	2.5×10^{-5}/2.6×10^{-6}	1.9/1.7	0.6/0.6	1.1/0.8
CdSx1	685	31.0/34.3	75.6	16.1	8.7×10^{-7}/4.6×10^{-7}	1.5/1.5	0.6/0.6	0.8/0.5
ZnOSx1/2	692	30.1/33.3	74.2	15.5	1.6×10^{-6}/4.6×10^{-7}	1.6/1.5	0.4/0.5	1.9/1.1
CdSx1/2	693	26.5/30.2	77.3	14.2	8.6×10^{-7}/8.1×10^{-8}	1.6/1.4	0.8/0.9	0.6/0.3
ZnOSx1/6	666	20.7/22.9	68.7	9.5	3.0×10^{-6}/3.5×10^{-7}	1.6/1.5	0.6/0.6	3.4/2.0
CdSx1/6	672	16.7/19.3	74.6	8.3	1.4×10^{-6}/1.6×10^{-7}	1.6/1.4	0.2/0.3	0.7/0.3

The data for each sample are obtained from one of the best cells of that sample. J_{sc} values calculated by integrating the measured IQE curves [see Fig. 3(a)] with the AM 1.5 spectrum are shown for comparison. One-diode parameters fitted from light and dark *J-V* measurements on those cells are shown as well.

with lower bandgap, toward the undoped ZnO layer. Such a bilayer is applied since a sulfur rich surface has been found experimentally in the work by Platzer–Björkman *et al.* [30]. The difference in band gap of these layers can be observed in the band diagram of Fig. 2(b). Total Zn(O,S) buffer layer thickness was chosen as 25 nm, as estimated in [14]. Zn(O,S) band gap values and conduction band offsets (CBOs) between the Zn(O,S) layers as well as toward the CIGS layer are taken from [30]. The Zn(O,S) doping level was selected by fitting the *J–V* measurements and is similar to what was found by Hall measurements on ZnO-based ALD buffers in [31]. In order to reproduce the slightly lower V_{oc} of the Zn(O,S) devices in comparison to the CdS references, a slightly higher interface donor defect density is assumed in the Zn(O,S) cell models.

III. RESULTS

A. Measurements

Measured *J–V* parameters, including the efficiency η, are shown in Table III. For each sample the table shows data for one of the best cells.

V_{oc} and FF increase when reducing the thickness of the absorber to half of its standard value. Further reduction does, however, lead to a significant decrease in V_{oc} as well as FF. In general, CdS references have higher V_{oc} and FF than corresponding Zn(O,S) samples.

There is a consistent decrease in J_{sc} when reducing the CIGS thickness. This loss in current is associated with a reduction in spectral response that is most severe at long wavelengths as seen in Fig. 3(a). The dotted curves represent the internal quantum efficiency (IQE) calculated from the measured zero bias EQE and the total reflectance of the solar cell stacks. Zn(O,S) buffer layers give devices with higher J_{sc} than CdS buffers. This is mainly due to the higher band gap of Zn(O,S) resulting in less UV and blue light absorption in the buffer. This effect is clearly seen in Fig. 3(a) as an improved IQE at short wavelengths. For the thinner samples, there is also a gain in the response at long wavelengths when exchanging CdS with Zn(O,S) as the buffer layer. Current density values obtained by integrating the measured IQE curves are also displayed in Table III. No significant voltage dependent current collection is seen for reverse bias EQE measurements.

The efficiency trend is negative when thinning the absorber layer, but devices with Zn(O,S) buffers outperform the CdS reference devices at these thicknesses.

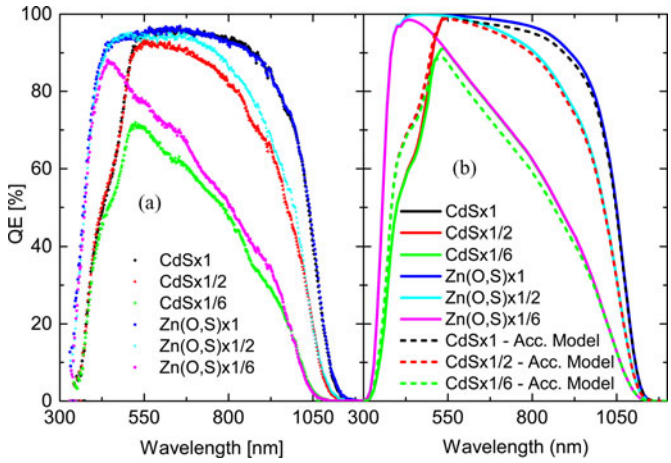

Fig. 3. Measured and simulated internal quantum efficiency curves. Measurements are shown as scattered plots in (a) while solid and (b) dashed lines represent simulated data. Dashed lines show IQE-curves for the CdS models with acceptor defects pinning the Fermi-level close to the CIGS valence band, at the buffer–absorber interface.

TABLE IV
MEASURED DEPLETION WIDTHS W, AND ACTIVATION ENERGIES, E_{act}, OF THE DIFFERENT SAMPLES

Sample	**w(v=0)** µm	**E_{act}** eV
ZnOSx1	0.20	1.23
CdSx1	0.21	1.18
Zn(O,S)x1/2	0.20	1.28
CdSx1/2	0.16	1.27
Zn(O,S)x1/6	0.21	1.32
CdSx1/6	0.17	1.30

Depletion widths were extracted at zero voltage bias from *CV* measurement sweeps conducted at 300 K. Activation energies were extrapolated from the temperature-dependence of V_{oc}.

Additionally Table III show one-diode parameters, of the same cells, fitted from light and dark *J–V* curves using the method developed in [32]. These parameters are the saturation current density J_0, the shunt conductance G_{sh}, the series resistance R_s, and the ideality factor A. Zn(O,S) cells generally have higher J_0 and G_{sh} than the CdS devices. These differences contribute to the lower FF of the cells with Zn(O,S) buffers.

CV profiles acquired at 150 K indicate doping concentrations in the range of 1×10^{16}cm^3 to 1×10^{17}cm^3. Depletion widths calculated at zero bias from measurements at 300 K are shown in Table IV. For the samples of standard thickness, widths are

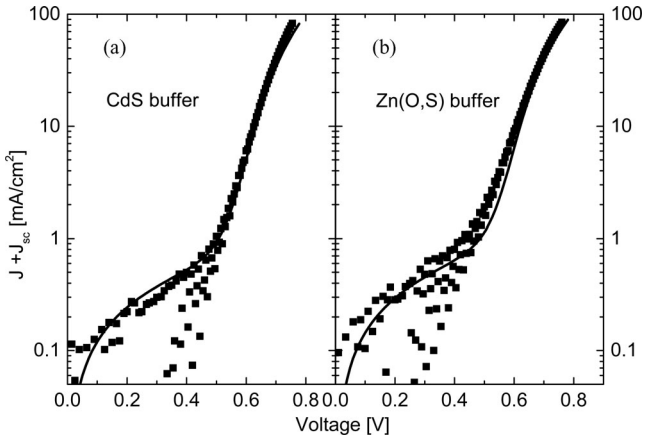

Fig. 4. Comparison of simulated (line) and measured (points) light curves for cells with 1.6 μm thick absorbers. CdS and Zn(O,S) buffered cells are shown in (a) and (b), respectively. Current density data are shown on logarithmic scale, shifted with $J_{\rm sc}$. Outliers are due to noise in the measurements.

TABLE V
JV PARAMETERS RESULTING FROM DEVICE SIMULATIONS

Model	V_{oc} [mV]	J_{sc}(IQE) [mA cm^{-2}]	FF [%
ZnOSx1	700	38.6	74.4
CdSx1	705	36.3	75.0
Zn(O,S)x1/2	714	36.1	77.1
CdSx1/2	726	33.8	76.9
Zn(O,S)x1/6	709	27.9	72.6
CdSx1/6	720	25.7	78.5

R_s and $G_{\rm sh}$ values of Table III are accounted for in SCAPS.

similar regardless of buffer layer, while for thinner absorbers, narrower depletion widths are obtained for the CdS devices.

From measured *J–V* curves at different temperatures, activation energies were extracted by linear extrapolation of $V_{\rm oc}$, at temperatures of 230 K and above, toward 0 K. Activation energies obtained from good cells are shown in Table IV. These values are in the range of the CIGS bandgap and are therefore an indication of recombination in the CIGS layer limiting $V_{\rm oc}$ [33]. There is a trend of increasing activation energy when thinning the CIGS layer.

B. Simulations

In Fig. 4, simulated *J–V* curves are compared with *J–V*curves measured on cells of standard thickness. *J–V* parameters resulting from the device models with donor interface defects are shown in Table V. R_s and $G_{\rm sh}$ values of Table III were accounted for in the simulations. As seen when comparing Tables III and V, simulations give higher $V_{\rm oc}$ and $J_{\rm sc}$ values than measurements. In some cases also the FF is significantly higher in simulations. Trends in the *J–V* parameter are rather well reproduced. As in measurements, $V_{\rm oc}$ is higher while $J_{\rm sc}$ is lower for cells with CdS buffer compared with cells with Zn(O,S) as a buffer layer. In agreement with measurements, the highest $V_{\rm oc}$ values are obtained with the medium thick CIGS layer, while there is a loss in $V_{\rm oc}$ when reducing the CIGS layer thickness from 0.85 to 0.3μm. However, the lower $V_{\rm oc}$ for the 0.3 μm case as compared with standard thickness seen in measurements is not reproduced in simulations. This could be due to a slightly worse material quality of the thin CIGS, not taken into account in simulations.

In all models, $V_{\rm oc}$ is limited by recombination in the CIGS layer. This is in correspondence with the measured activation energies of Table IV. When thinning the CIGS layer, the total recombination decreases, which leads to an improvement of the $V_{\rm oc}$. The improvement is stronger than measured for the CdS cells, while for the Zn(O,S) cells, it is on par with measurements. A thinner absorber layer does, however, also lead to an increase in electron density due to more light absorption close to the back contact. The effect of more recombination close to and at the back contacts counteracts the positive effect of reducing the CIGS thickness. The assumption of a defect rich region close to the back contact strengthens this negative effect. Eventually, the total recombination increases when thinning the CIGS layer and this results in a $V_{\rm oc}$ loss, which we indeed observe when the CIGS thickness is reduced from 0.8 to 0.3μm. In the thinner devices, a larger fraction of recombination occurs in regions where the band gap is relatively high. In this graded CIGS layer, the bandgap near the back contact is up to 1.3 eV. This could explain the increase in the activation energy observed when thinning the absorber layer (see Table IV). The slightly lower $V_{\rm oc}$ values observed in measurements on Zn(O,S) cells in comparison to those of the CdS devices, are reproduced in simulations.

Fig. 3 shows measured and simulated IQE curves. The shape of the curves are similar, but the IQE level is generally higher in simulations than in measurements. This is true even for the thickest cells. Most prominent are, however, the IQE differences for thinner samples, especially those with CdS buffers. These discrepancies correspond to current densities from 20 to $6.5\,{\rm mA}\cdot{\rm cm}^{-2}$ as seen when comparing the current values of Table V with $J_{\rm sc}$ values from measured IQE shown in Table III. Such differences between measurements and simulations were found in [10], also for the thickest absorber layers, where they were attributed to inactive areas in the CIGS films.

To model the difference in IQE levels at long wavelengths between thin CdS and Zn(O,S) devices a significant difference in the CIGS band-bending is required. This is in correspondence with the difference in depletion widths obtained from the CV measurements of Table IV. As briefly mentioned before, the lower potential drop in CIGS is in this study achieved using a high density of acceptor defects at the CdS–CIGS interface at an energy level corresponding to a low level in the CIGS band gap. Assuming these interface properties while keeping the same CIGS bulk properties as in the previous model, a relatively good correspondence to the measured IQE difference can be obtained. The cross sections of these acceptors are assumed very low in order to cause pinning of the Fermi level while avoiding interface recombination at the absorber–CdS interface. The adjusted model is denoted the acceptor model in Table II as well as in Figs. 2(a) and 3(b). As is clearly visible in Fig. 2(a), a major part of the band bending occurs in the CdS layer for the acceptor model. This leads to a better collection from the CdS layer as seen from the simulated IQE-curves at short wavelengths. No voltage dependent current collection at long wavelengths is seen

for this model, which is in agreement with our measurement results. A side effect of the acceptor pinning is, however, a slight voltage-dependent current collection at short wavelengths. We have observed such a behavior for some CIGS solar cells with CdS buffer previously.

In contrast with what is seen in the measurements of Fig. 3.(a), there is in simulations also a clear difference in long wavelength collection between the acceptor model and the Zn(O,S) model for the thickest devices. An enhanced EQE at these wavelengths has previously been observed by us for Cd-free devices of standard thickness as compared with CdS reference cells. The fact that we do not observe such a buffer-dependent difference for the standard devices in this study could be related to their comparable depletion widths (see Table IV).

IV. Discussion

CIGS cells fabricated in this study are of high quality. The efficiencies of the thin CdS buffered cells are in line with those obtained in other work on CdS cells with thin absorbers [1], [4]. The thin Zn(O,S) devices processed here have efficiencies exceeding their CdS references.

J–V parameters are in almost all cases higher in simulations than in measurements. This indicates that the models are more ideal than the real cells. The largest relative differences are for $J_{\rm sc}$ of the thinnest cells, especially for those with a CdS buffer. The same holds for the $J_{\rm sc}$ values obtained from integrating the IQE-curves, shown in Tables III and V. It is fairer to compare the simulated values with the measured IQE values of Table III than the *J–V* values of the same table. The *J–V* values arise from EQE-calibrated measurements. The large loss in $J_{\rm sc}$ for the thin devices could be due to consistently worse and more inhomogeneous electrical properties, which is not accounted for in the models. From 4 to 11 mV of the observed $V_{\rm oc}$ differences could be explained by the difference in $J_{\rm sc}$ between simulated and measured *J–V*curves. The rest of the $V_{\rm oc}$ difference must be due to some other limitation of the models.

We observe that the depletion region widths for the cells with CdS buffer layers vary with respect to CIGS thickness. The interface acceptors, proposed to reduce the CIGS band-bending of the CdS cells in this study, might be related to the air exposure prior to the CBD process as well as to the CBD process itself. The ALD of the Zn(O,S) is performed without breaking vacuum after the CIGS deposition. Furthermore, based on the varying depletion width, there seems to be a dependence on the CIGS thickness for these defects. We propose two thickness related factors that perhaps could affect the defect distributions. These factors are that the steepness in the Ga-grading inherent from the in-line deposition process varies with CIGS thickness and additionally that the time in the deposition zone varies with the process speed and thereby the layer thickness.

A positive CBO between the CIGS and the CdS could function as a barrier to the light-generated current. However, the positive CBO of the acceptor model, visible in Fig. 2(a), does not cause such an effect in the simulations. This barrier is thin enough to let electrons pass by tunnelling. The value of the offset is not well defined. Everything from a negative CBO to high positive one has been measured for CIGS–CdS interfaces (see [20]).

Another possible source of the higher IQE-level measured on the thin Zn(O,S) cells could be a higher optical absorption in these samples. Reflection and transmission measurements on the stacked films without back contact do, however, not give any indication of a buffer related difference in optical absorption.

In order to increase the understanding of the devices, it might be useful to study material variations in two or three dimensions. Furthermore, material and device characterization could be combined with optical and electrical modeling in more than one dimension. It would also be good to know the real depth composition as well as the doping of the Zn(O,S) layer. The sulfur gradient is in reality continuous but exactly how it varies is not clear. One way to improve the Zn(O,S) devices might be to lower $G_{\rm sh}$ by using a slightly thicker undoped ZnO layer.

V. Conclusion

CIGS solar cells with absorbers of three different thicknesses and buffers of two types, Zn(O,S) and CdS, are fabricated. Devices are characterized by optical and electrical measurements and the results are compared with 1-D device simulations.

High efficiencies are obtained for standard ($\eta \approx 16\%$) as well as thinner than standard devices, with a thickness down to 0.3 μm ($\eta \approx 9\%$). Cells with 0.8 to 0.9 μm thick absorber layers show the highest $V_{\rm oc}$ and FF while, due to the high $J_{\rm sc}$, the highest efficiencies are found for standard devices with 1.6 μm absorbers. For absorbers of this thickness Zn(O,S) and CdS devices are of comparable efficiency. Thinner Zn(O,S) cells are significantly more efficient than CdS reference devices of corresponding thickness, due to the much higher $J_{\rm sc}$. Trends in measured *J–V* and IQE curves can, to a large extent, be reproduced in simulations. Devices are limited by recombination in the CIGS layer. Recombination at the back contact gains in importance when thinning the absorber layer.

A better IQE is observed both at short and long wavelengths for the thinner Zn(O,S) devices. Below 500 nm there is less light absorption in Zn(O,S) than in CdS. We propose that the difference at longer wavelength is caused by a difference in CIGS band-bending and a poor back contact region. The difference in band-bending may be associated with acceptor defects at the CdS–CIGS interface.

Acknowledgment

The authors would like to thank B. Vermang for providing back reflection data.

References

[1] O. Lundberg, M. Bodegård, J. Malmström, and L. Stolt, "Influence of the Cu(In,Ga)Se_2 thickness and Ga grading on solar cell performance," *Progr. Photovolt., Res. Appl.*, vol. 11, no. 2, pp. 77–88, 2003.

[2] T. Negami, S. Nishiwaki, Y. Hashimoto, N. Kohara, and T. Wada, "Effect of absorber thickness on performance of Cu(In,Ga)Se_2 solar cells," in *Proc. 2nd World Conf. Photovolt. Energy Convers.*, Piscataway, NJ, USA, 1998, pp. 1181–1184.

[3] K. Orgassa, H. W. Schock, and J. H. Werner, "Alternative back contact materials for thin film Cu(In,Ga)Se_2 solar cells," *Thin Solid Films*, vol. 431–432, pp. 387–391, May 2003.

[4] K. Ramanathan, R. Noufi, B. To, D. Young, R. Bhattacharya, M. Contreras, R. Dhere, and G. Teeter, "Processing and properties of sub-micron CIGS solar cells," in *Photovolt. Energy Convers., Conf. Rec., IEEE 4th World Conf.*, May 2006, vol. 1, pp. 380–383.

[5] W. Shafarman, R. Birkmire, S. Marsiliac, M. Marudachalam, and N. Orbey Russell, "Effect of reduced deposition temperature, time and thickness on cu(in,ga)se2 films and devices," in *Proc. 26th IEEE Photovoltaic Solar Energy Conf. Exhib.*, Anaheim, CA, USA, 1997, pp. 331–334.

[6] J. Malmström, O. Lundberg and L. Stolt, "Potential for light trapping in $Cu(In,Ga)Se_2$ solar cells," in *Proc. IEEE 3rd World Conf. Photovolt. Energy Convers*., 2003, pp. 344–347.

[7] A. Čampa, J. Krč, M. Edoff, F. Smole, and M. Topič, "The potential of textured front ZnO and flat TCO/metal back contact to improve optical absorption in thin $Cu(In,Ga)Se_2$ solar cells," *Thin Solid Films*, vol. 515, no. 15, pp. 5968–5972, May 2007.

[8] N. Dahan, Z. Jehl, T. Hildebrandt, J.-J. Greffet, J.-F. Guillemoles, D. Lincot, and N. Naghavi, "Optical approaches to improve the photocurrent generation in $Cu(In,Ga)Se_2$ solar cells with absorber thicknesses down to 0.5 μm," *J. Appl. Phys*., vol. 112, no. 9, pp. 094902-1–094902-7, 2012.

[9] F. Erfurth, Z. Jehl, M. Bouttemy, N. Dahan, P. Tran-Van, I. Gerard, A. Etcheberry, J.-J. Greffet, M. Powalla, G. Voorwinden, D. Lincot, J. Guillemoles, and N. Naghavi, "Mo/$Cu(In, Ga)Se_2$ back interface chemical and optical properties for ultrathin CIGSe solar cells," *Appl. Surf. Sci*., vol. 258, no. 7, pp. 3058–3061, 2012.

[10] M. Gloeckler and J. R. Sites, "Potential of submicrometer thickness $Cu(In,Ga)Se_2$ solar cells," *J. Appl. Phys*., vol. 98, no. 10, pp. 103703-1–103703-7, 2005.

[11] M. Burgelman, P. Nollet, and S. Degrave, "Modelling polycrystalline semiconductor solar cells," *Thin Solid Films*, vol. 361–362, pp. 527–532, 2000.

[12] C. Platzer-Björkman, J. Kessler and L. Stolt, "Atomic layer deposition of Zn(O,S) buffer layers for high efficiency Cu(In,Ga)Se2 solar cells," in *Proc. 3rd World Conf. Photovolt. Energy Convers*., Osaka, Japan, 2003, pp. 461–464.

[13] J. Kessler, M. Bodegård, J. Hedström, and L. Stolt, "Baseline $Cu(In,Ga)Se_2$ device production: Control and statistical significance," *Solar Energy Mater. Solar Cells*, vol. 67, no. 1–4, pp. 67–76, 2001.

[14] U. Zimmermann, M. Ruth, and M. Edoff, "Cadmium free CIGS minimodules with ald-grown Zn(O,S)-based buffer layers," in *Proc. 21st Eur. Photovolt. Solar Energy Conf*., Dresden, Germany, 2006, pp. 1831–1834.

[15] M. Edoff, S. Woldegiorgis, P. Neretnieks, M. Ruth, J. Kessler, and L. Stolt, "CIGS submodules with high performance and high manufacturability," in *Proc. 19th Eur. Photovolt. Solar Energy Conf*., Paris, France, 2004, pp. 1690–193.

[16] A. Hultqvist, C. Platzer-Björkman, E. Coronel, and M. Edoff, "Experimental investigation of $Cu(In_{1-x},Ga_x)Se_2/Zn(O_{1-z},S_z)$ solar cell performance," *Solar Energy Mater. Solar Cells*, vol. 95, no. 2, pp. 497–503, 2011.

[17] J. Pettersson, M. Edoff, and C. Platzer-Bjorkman, "Electrical modeling of $Cu(In,Ga)Se_2$ cells with ALD-$Zn_{1-x}Mg_xO$ buffer layers," *J. Appl. Phys*., vol. 111, no. 1, pp. 014509-1–014509-11, 2012.

[18] J. Pettersson, C. Platzer-Björkman, U. Zimmermann, and M. Edoff, "Baseline model of graded-absorber $Cu(In,Ga)Se_2$ solar cells applied to cells with $Zn_{1-x}Mg_xO$ buffer layers," *Thin Solid Films*, vol. 519, no. 21, pp. 7476–7480, 2011.

[19] S. Schleussner, J. Pettersson, T. Törndahl, and M. Edoff, "Surface engineering in $Cu(In,Ga)Se_2$ solar cells," *Progr. Photovolt., Res. Appl*., vol. 21, no. 4, pp. 561–568, 2013.

[20] J. Pettersson. (2012). "Modelling band gap gradients and Cd-free buffer layers in $Cu(In,Ga)Se_2$ solar cells," Ph.D. dissertation, Uppsala Univ., [Online]. Available: http://urn.kb.se/resolve?urn=urn:nbn:se:uu:diva-168618

[21] K. Orgassa, U. Rau, H. Schock, and J. Werner, "Optical constants of $cu(in,ga)se_2$ thin from normal incidence transmittance and reflectance," in *Proc. 3rd World Conf. Photovolt. Energy Convers*., Osaka, Japan, 2003, pp. 2P–A8–04.

[22] K. Orgassa, "Coherent optical analysis of the ZnO/CdS/$Cu(In,Ga)Se_2$ thin film solar cell," Ph.D. dissertation, Inst. Photovoltaik, Univ. Stuttgart, Stuttgart, Germany, 2004.

[23] A. Hultqvist, C. Platzer-Björkman, T. Törndahl, M. Ruth, and M. Edoff, "Optimization of i-zno window layers for cu(in,ga)se2 solar cells with ald buffers," in *Proc. 22nd Eur. Photovolt. Solar Energy Conf*., Milan, Italy, 2007, pp. 2381–2384.

[24] M. I. Alonso, M. Garriga, C. A. Durante Rincón, E. Hernández, and M. León, "Optical functions of chalcopyrite $CuGa_xIn_{1-x}Se_2$ alloys," *Appl. Phys. A, Mater. Sci. Process*., vol. 74, pp. 659–664, 2002.

[25] W. N. Shafarman and L. Stolt, "$Cu(In,Ga)Se_2$ solar cells," in *Handbook of Photovoltaic Science and Engineering*, A. Luque and S. Hegedus, Eds. New York, NY, USA: Wiley, 2003, ch. 13, pp. 567–616. [Online]. Available: http://www.knovel.com/web/portal/browse/

[26] G. Hanna, A. Jasenek, U. Rau, and H. Schock, "Influence of the Ga-content on the bulk defect densities of Cu(In,Ga)Se2," *Thin Solid Films*, vol. 387, no. 1–2, pp. 71–73, 2001.

[27] A. Jasenek, U. Rau, V. Nadenau, and H. W. Schock, "Electronic properties of $CuGaSe_2$-based heterojunction solar cells—Part II: Defect spectroscopy," *J. Appl. Phys*., vol. 87, no. 1, pp. 594–602, 2000.

[28] T. Eisenbarth, T. Unold, R. Caballero, C. A. Kaufmann, and H.-W. Schock, "Interpretation of admittance, capacitance-voltage, and current-voltage signatures in $Cu(In,Ga)Se_2$ thin film solar cells," *J. Appl. Phys*., vol. 107, no. 3, pp. 034509-1–034509-12, 2010.

[29] F. Duerinckx, I. Kuzma-Filipek, K. Van Nieuwenhuysen, G. Beaucarne, and J. Poortmans, "Simulation and implementation of a porous silicon reflector for epitaxial silicon solar cells," *Progr. Photovolt., Res. Appl*., vol. 16, no. 5, pp. 399–407, 2008.

[30] C. Platzer-Bjorkman, T. Torndahl, D. Abou-Ras, J. Malmstrom, J. Kessler, and L. Stolt, "Zn(O,S) buffer layers by atomic layer deposition in $Cu(In,Ga)Se_2$ based thin film solar cells: Band alignment and sulfur gradient," *J. Appl. Phys*., vol. 100, no. 4, pp. 044506-1–044506-9, 2006.

[31] J. Pettersson, C. Platzer-Björkman, A. Hultqvist, U. Zimmermann, and M. Edoff, "Measurements of photo-induced changes in the conduction properties of ALD-$Zn_{1-x}Mg_xO$ thin films," *Physica Scripta*, vol. 2010, no. T141, pp. 014010-1–014010-4, 2010.

[32] S. Hegedus and W. N. Shafarman, "Thin-film solar cells: Device measurements and analysis," *Progr. Photovolt., Res. Appl*., vol. 12, no. 2–3, pp. 155–176, 2004.

[33] U. Rau and H.-W. Schock, "Electronic properties of $Cu(In,Ga)Se_2$ heterojunction solar cells—Recent achievements, current understanding, and future challenges," *Appl. Phys. A (Mater. Sci. Process.)*, vol. A69, no. 2, pp. 131–47, 1999.

Authors' photographs and biographies not available at the time of publication.